

phys. stat. sol. (b) **216**, 291 (1999)

Subject classification: 78.66.Fd; 71.35.Cc; 78.47.+p; 78.55.Cr; S7.14; S7.15

Optical Spectroscopy of InGaN/GaN Quantum Wells

E. BERKOWICZ (a), D. GERSHONI (a), G. BAHIR (a), A.C. ABARE (b),
S.P. DENBAARS (b), and L.A. COLDREN (b)

(a) *The Solid State Institute, Technion-Israel Institute of Technology, Haifa, 32000, Israel*
e-mail: dg@physics.technion.ac.il

(b) *Department of Electrical and Computer Engineering, University of California,
Santa Barbara, California 93106, USA*

(Received July 4, 1999)

We apply photoluminescence, photoluminescence excitation and time-resolved optical spectroscopy for studying a well-characterized set of InGaN/GaN periodic structures. The energy differences between the absorption edge and the photoluminescence peak and the photoluminescence decay times drastically increase with the InGaN quantum well thickness. We quite accurately determined the radiative and non-radiative decay times of excitons in these structures from the measured decay times, the integrated photoluminescence intensity and the photoluminescence intensity immediately after the excitation pulse, at various temperatures. The intrinsic radiative lifetimes, which are inversely proportional to the exciton oscillator strengths, are then calculated from the temperature dependence of the radiative lifetimes. These experimental findings are analyzed using an eight-band $\mathbf{k} \cdot \mathbf{P}$ model, which quantitatively explains both the Stokes shifts and the intrinsic radiative lifetimes. Their strong dependence on the quantum well width is due to a strong lattice-mismatch strain induced piezoelectric field along the growth axis.

1. Introduction

Considerable progress in the hetero-epitaxy of group-III nitrides using low temperature deposited buffer layers [1–3] have recently led to the demonstration of new devices operating in the ultra violet (UV) spectral range. In most of these devices [4] InGaN quantum well (QW) layers embedded within GaN barrier layers are acting as the active layer. Therefore, the properties of this material system have become a subject of intensive research efforts. Key issues in these studies are: (i) The value of the optical band-gap and its composition and strain dependence. (ii) The reason for the large difference between the absorption and the emission spectrum (Stokes shift) and (iii) the recombination dynamics of excitons and free carriers in these heterostructures.

Large lattice-mismatch strain fields which lead to the presence of large piezoelectric fields, large density of dislocations, interface roughness, composition fluctuations and even a complete phase separation [5, 6], are reported to drastically affect the optical properties of these heterostructures.

In this paper, we report on continuous wave (cw) and pulsed, temperature dependent, photoluminescence (PL) spectroscopy of a set of InGaN/GaN multi-quantum-well (MQW) samples which were carefully characterized by high-resolution X ray diffraction (HRXRD). We show that a strong lattice-mismatch strain induced piezoelectric field along the growth axis largely determines the optical properties of these heterostructures.

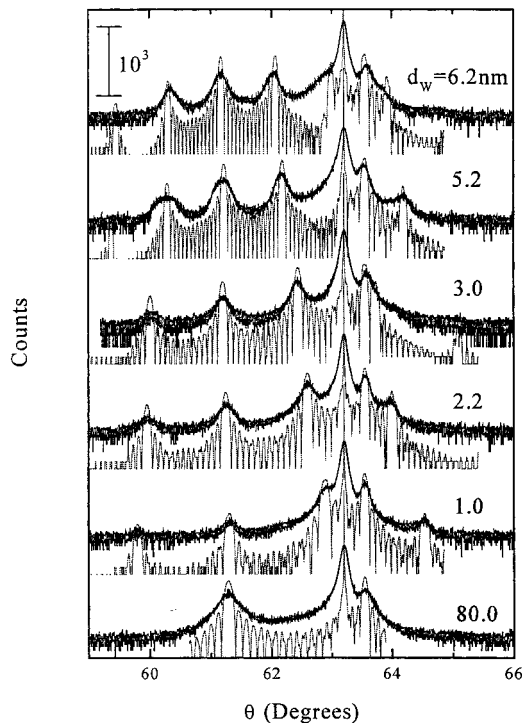


Fig. 1. Measured and calculated HRXRD scans for the six studied InGaN/GaN heterostructures

2. Samples

The InGaN/GaN samples were grown on *c*-plane sapphire substrates by atmospheric pressure MOCVD using trimethylgallium, ammonia, disilane, and trimethylindium, as precursors. A 19 nm thick GaN nucleation layer was first deposited at 525 °C. A 2.5 μm thick buffer layer of GaN was then deposited at 1050 °C. In five samples, a multi quantum well (MQW) structure consisting of 14 periods were then grown on the GaN buffer layer at a temperature of 790 °C. Each period consisted of a nominally $2 \times 10^{18} \text{ cm}^{-3}$ Si doped 4.6 nm thick GaN barrier and a layer of $\text{In}_{0.1}\text{Ga}_{0.9}\text{N}$ (QW). In an additional control sample an 80 nm thick layer of

$\text{In}_{0.1}\text{Ga}_{0.9}\text{N}$ was deposited in place of the MQW. A 112 nm thick $\text{Al}_{0.06}\text{Ga}_{0.94}\text{N}$ cap layer concluded the sample growth.

We used high-resolution X-ray reciprocal space mapping [7, 8] in the vicinity of the (105) asymmetric reflection in order to determine the strain state of our heterostructures. All the samples, including the control sample, were found to be fully strained. The layer compositions and their dimensions were determined by HRXRD in the vicinity of the (006) symmetric reflection. The data were obtained from triple-axis scans as shown in Fig. 1, together with the diffraction simulations.

The deduced InGaN layer thicknesses are indicated in Fig. 1.

3. Band Structure Calculations

In order to calculate the energy band structure and the optical properties of these heterostructures we used an eight-band $\mathbf{k} \cdot \mathbf{P}$ Kane-Luttinger-like Hamiltonian modified to take into account the reduced symmetry of the wurtzite structure [9]. Our model calculations proceed along the lines described by Baraff and Gershoni [10]. Compiled material bulk parameters [9] were used for each region and the effect of the strain was introduced to the Hamiltonian by the use of a phenomenological deformation potential theory with bulk deformation potentials. Piezoelectric fields were introduced into the Hamiltonian in a procedure described by Pistol and Gershoni [11]. We used a Fourier expansion method to convert the eight-coupled differential equations into a matrix eigenvalue problem, which is then solved numerically. The piezoelectric constants, which actually determine the absolute magnitude of the piezoelectric field, are used in this

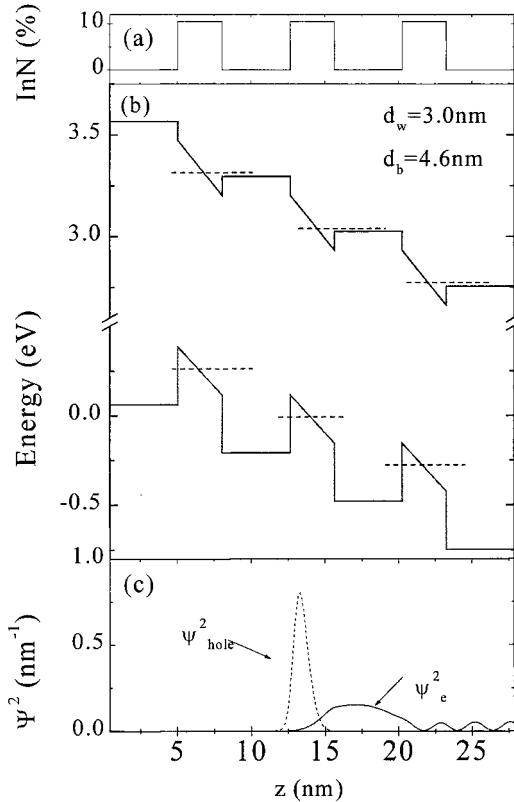


Fig. 2. a) Heterostructure growth sequence, b) potential structure, and c) probability of carrier distributions

work as an adjustable parameter to best fit the measurements. The magnitude of the piezoelectric constant thus obtained is smaller than those reported in the literature. Probably due to the presence of polarization fields [12] and due to electric field screening by the presence of carriers [13].

In Fig. 2a we schematically describe three periods of one of the MQW samples. In Fig. 2b we depict the resultant potential structure for electron and hole in the lowest conduction band and highest valence band, respectively. The calculated probability distributions of these carriers are shown in Fig. 2c.

4. Optical Studies

For the optical measurements the samples were mounted in a closed-circuit helium flow optical cryostat. We used a xenon lamp and a 0.34 m monochromator as the light source for the PL excitation (PLE) measurements. For the time-resolved spectroscopy the samples were excited by a frequency-doubled picosecond pulsed radiation from a Ti:sapphire laser. The collected PL light was dispersed by a 0.22 m monochromator and detected by either a UV enhanced liquid nitrogen cooled charge coupled device (CCD) in the cw detection mode, or by a multi channel plate cooled photomultiplier in the time correlated single photon counting mode.

In Fig. 3 we present the low temperature PL and PLE spectra of the samples. The spectrally integrated PL intensity was found to be linear with the excitation density over four orders of magnitude around 500 W/cm². We note that the PL lines are rather wide, their full spectral width at half the line maximum (FWHM) amounts to 60 to 80 meV. These broad linewidths are due to inhomogeneous broadening as a result of potential fluctuations due to composition fluctuations, strain fluctuations, interface roughness, and crystalline dislocations and defects. We observed some variations in the PL spectral shape and integrated intensity as a function of the beam position on the sample, indicative of their non-uniformity. As expected, the wider the QWs are the lower is their PL emission energy. This dependence can only be partially accounted for by the quantum size effect.

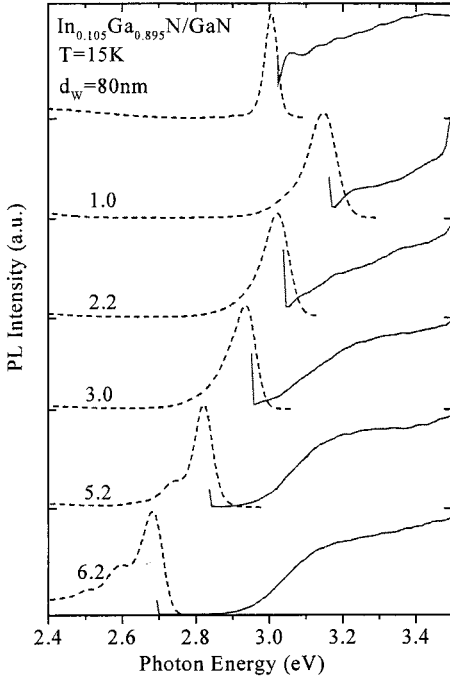


Fig. 3. PL (dashed lines) and PLE (solid lines) spectra of the InGaN/GaN heterostructures

The PLE spectra in Fig. 3 were normalized to unity at their maximum, right below the bandgap of the AlGaIn cap layer. The absorption edge as determined by the PLE spectra, follows the PL peak and it also shifts to lower energies as the well width increases. In addition, it can be seen that the energy difference between the absorption edge and the PL peak increases with the well width. The oscillator strength for the optical transition, as determined from the strength of the absorption edge, significantly decreases with the QW width. Our model, which assumes a piezoelectric field of 900 kV/cm as shown in Fig. 2, quite nicely mimics these features of the measured PLE spectra as can be seen by comparison with the calculated absorption spectra of Fig. 4.

An excitonic resonance in the PLE spectrum of the control sample is clearly observed at the absorption edge. Only a small resonance is observed in the PLE spectrum of the narrowest MQW sample, and it is absent in the spectra of the wider MQW samples. Our model calculations do not include the excitonic effect. However, its absence from the PLE spectra of the wider MQW samples can be readily understood in terms of the decrease in the overlap integral between the electron and hole wavefunctions, yet another consequence of the presence of the large piezoelectric field. Consequently, its presence in the ‘bulk’ layer is indicative of a much smaller field there. This is probably due to large spatial scale redistribution of the extrinsic charges which compensates the piezoelectric field. We note here that the maximum possible built-in field in an intrinsic, 80 nm thick $\text{In}_{0.1}\text{Ga}_{0.9}\text{N}$ layer cannot exceed 300 kV/cm, a factor of three smaller than the estimated piezoelectric field in the MQW layers.

In Fig. 5 we show the spectrally integrated PL intensity as a function of sample temperature for all the studied samples. The intensity is normalized at the lowest measured temperature (15 K). The decrease in the PL intensity with temperature clearly indicates that the relative importance of the non-radiative recombination processes increases with the temperature. The rate at which the PL intensity decreases with temperature, increases with the QW width.

In general, a single exponent decay model did not faithfully describe the measured PL decay transients [14]. By comparing single exponent decay fits with two exponent decay fits we found that more than 90% of the temporally integrated PL emission could be described by a single exponential decay model. Therefore, we used single exponent decay curves for extracting one characteristic decay time for each PL decay measurement (not shown).

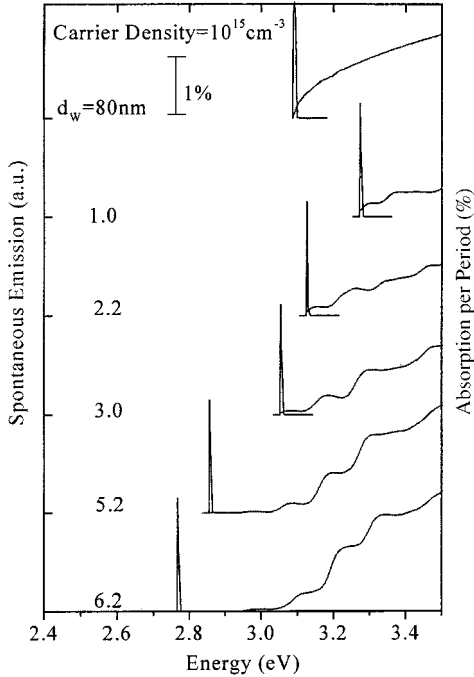


Fig. 4. Calculated emission (strong peaks) and absorption (solid line) spectra of the InGaN/GaN heterostructures

In Fig. 6 we display the fitted characteristic decay times at the PL peak as a function of temperature for the MQW samples. We observed that below 130 K, the decay transients of lower energies were longer and the decay transients of higher energies were shorter than those measured at the peak [14]. Above 130 K all the PL lines had one characteristic decay time. We attribute this behavior to a typical activation energy of 12 meV, which is required for carriers to leave their lateral potential fluctuation traps.

Two clear trends are readily observed in Fig. 6: First, we note that the broader the QWs are the longer are their PL decay times. In addition, we note that the PL effective lifetime increases with temperature up to 210, 240, 250 and 40 K for the 1.2, 2.5, 3.6, and 5.0 nm MQWs, respectively.

At higher temperatures, the effective PL lifetime starts to decrease with the sample temperature. For the 6.2 nm MQW and 80 nm bulk samples the decay times decrease with temperature already at 15 K. By comparison with similar studies performed on GaAs/GaAlAs MQW samples [15], we deduce that for the narrow MQW this behavior is due to thermionic emission of excitons from the QWs, which increases the non-radiative decay rate and thus effectively shortens τ_{eff}

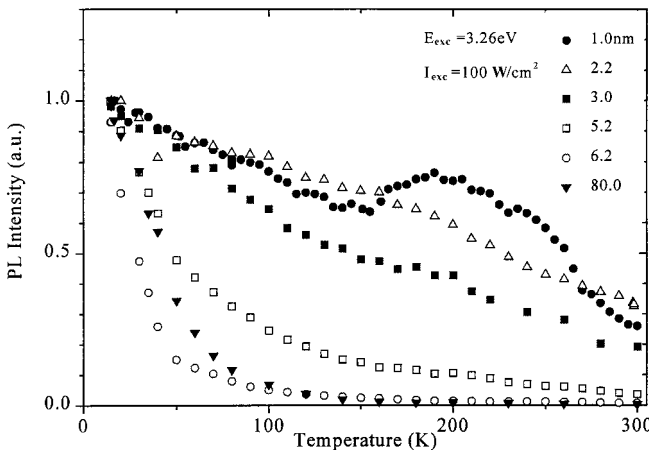


Fig. 5. Integrated PL intensity vs. sample temperature

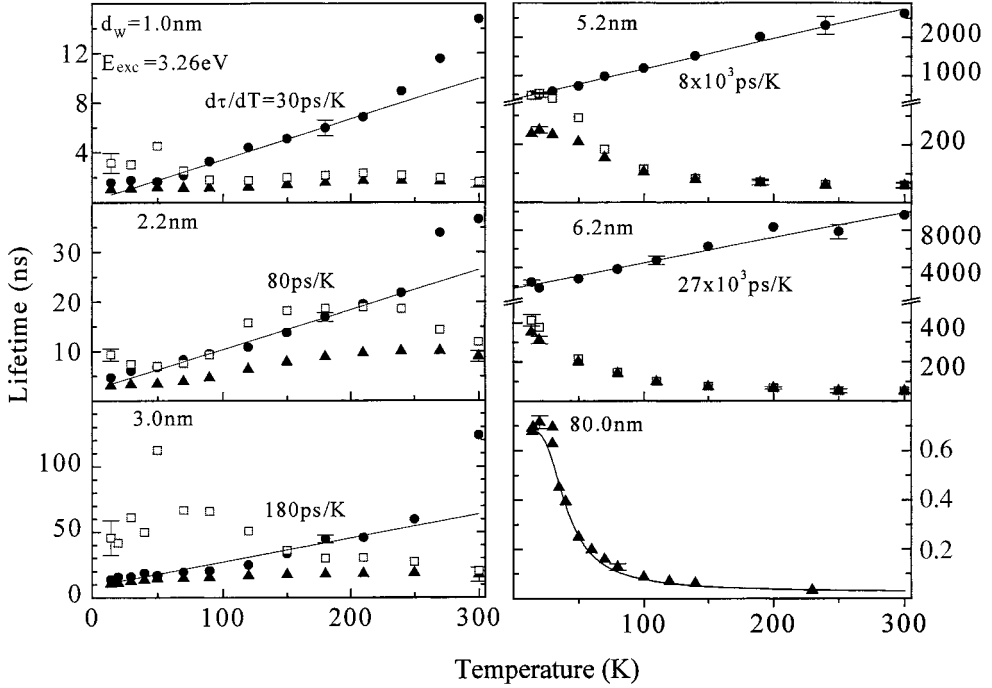


Fig. 6. The measured τ_{eff} (▲) and deduced lifetimes τ_{R} (●) and τ_{NR} (□) vs. sample temperature. The solid lines represent the fitted linear temperature dependence of τ_{R}

[16]. In the wider InGaN layers another process controls the non-radiative decay rates, as discussed below.

An important conclusion is readily made from the measured decay times of Fig. 6. In spite of the increasing importance of the non-radiative channels as the temperature rises (see Fig. 5), the transient characteristic decay times (τ_{eff}) are not becoming shorter. The overall recombination rate ($1/\tau_{\text{eff}}$) is the sum of the radiative decay rate ($1/\tau_{\text{R}}$) and the non-radiative one ($1/\tau_{\text{NR}}$). Since the latter can only increase with temperature, this means that the non-radiative rate is significantly smaller than the radiative one. We can thus safely conclude that at low temperatures the non-radiative decay rates are slower than the radiative ones for the four narrower MQW samples. With this information at hand, one can safely deduce that the radiative recombination lifetime (τ_{R}) is inversely proportional to the PL intensity at a given excitonic density. Thus, from the temperature dependence of the measured PL intensity during a short temporal window (which is significantly shorter than the effective lifetime) around the excitation time, one can directly measure the temperature dependence of the radiative lifetime. In Fig. 7 we display the reciprocal measured PL peak intensity during a time window of 200 ps immediately after the pulse excitation, as a function of the sample temperature. We note that between 70 and 250 K τ_{R} linearly increases with temperature. We checked our assumptions self-consistently by calculating for each temperature τ_{R} and τ_{NR} from the measured τ_{eff} and the PL intensity shortly after the excitation. From these times the integrated PL intensity is straightforwardly calculated and compared with the measured data as given in Fig. 5.

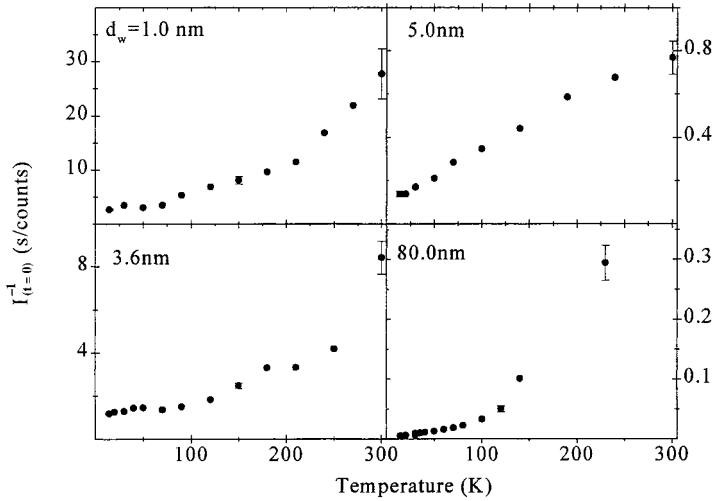


Fig. 7. The inverse of the maximum of the transient PL intensity vs. sample temperature

We display in Fig. 6 the deduced radiative and non-radiative lifetimes as a function of temperature for the MQW samples. We note that both the non-radiative and the radiative times are temperature dependent. While the first rapidly decreases with temperature, the latter, as already deduced from Fig. 6, linearly increases with temperature. Both times strongly increase with the quantum well width. The radiative times are temperature independent at lower temperatures. This is expected for fully localized excitons [17, 18]. Above 50 to 70 K, the radiative times increase linearly with the temperature up to around 250 K. This behavior is an unambiguous signature for a two dimensional (2D) excitonic system [19, 20]. In contrast, the radiative decay times of the 80 nm, control sample increase faster with temperature as expected for a 3D system. The effective PL lifetimes of the ‘bulk’ sample are much shorter than those of the MQW samples. They also decrease more rapidly with increasing sample temperature. We fitted the measured data with the activation model of Michler et al. [16]. According to this model carriers are trapped within potential fluctuations where they radiatively recombine. The decrease of the effective lifetime and the integrated PL intensity with increasing temperature is due to the thermal activation of these carriers out of their traps where non-radiative processes dominate the recombination. The fit, which is represented in Fig. 6 by the solid line, results in an activation energy of 13 meV, a radiative lifetime in the sub-nanosecond range, as deduced from Fig. 7 and an activated non-radiative lifetime of 20 ps.

5. Discussion

1. The main experimental results of our studies can be summarized as follows: The PL peak positions are spectrally red-shifted with increasing well width. These red-shifts are much larger than anticipated by considering the quantum confinement effect in symmetric QW structures.

2. There are large Stokes-like shifts between the band edge PL peaks and the absorption edge as measured by PLE. These shifts increase with increasing well width.

3. Only a very small excitonic resonance is observed in the absorption edge of very narrow InGaN QWs. The excitonic resonance is not observed at all in the absorption edge of wider QWs.

4. The spectral position of the PL peaks from wider MQW structures (well widths larger than 5 nm) is lower in energy than the PL peak energy from bulk InGaN layers.

5. The PL decay times rapidly increase with the InGaN QW width. This strong effect is much larger than expected for a symmetric QW structure.

6. The radiative lifetimes of carriers increase linearly with the sample temperature for temperatures above 50 to 70 K. Their temperature dependence rapidly increases with the QW width.

Two models have been recently proposed in the relevant literature to explain the optical properties of InGaN/GaN quantum structures: a) Carrier localization within low energy potential fluctuations due to the formation of In-rich areas or islands [5, 21]. b) The presence of large piezoelectric fields due to lattice-mismatch strain, which lead to the quantum-confined Stark effect [22, 23] Our measurements set an upper limit on the magnitude of the first assumption. We clearly show by temperature dependence time-resolved spectroscopy of MQW and bulk InGaN/GaN structures that these potential fluctuations amount to 10 to 15 meV only, while the PL spectral linewidths and Stokes shifts are an order of magnitude larger. In addition, we clearly show that the presence of the piezoelectric field largely determines the optical properties of these heterostructures.

In Fig. 8 we present the measured PL energies and the absorption edge as a function of the MQW widths. By the dashed line we display the calculated bandgap for these quantum systems assuming no piezoelectric field. We note that the difference between the calculated values and the measured ones, as well as the Stokes shifts linearly increase with the QW width. From this dependence, we quite accurately estimate the piezoelectric field which must be present along the growth direction of the InGaN strained QWs [3, 24]. Using the estimated piezoelectric field of 900 kV/cm we recalculate the MQW bandgap as shown by the solid line in Fig. 8 and the absorption spectra of Fig. 4. We note that the obtained agreements with the measurements are quite

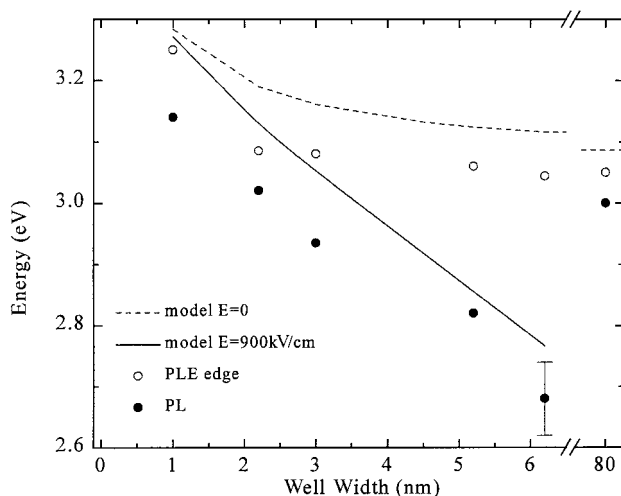


Fig. 8. PL energy (●) and PLE absorption edge (○) vs. QW width. The solid (dashed) line represents the calculated bandgap with (without) the piezoelectric field

good. In particular, the observation that the PL energies of the widest wells are below the calculated bulk InGaN bandgap (the dotted line in Fig. 8) is thus explained [22].

From the temperature range in which the radiative lifetime is linearly dependent on the temperature, we extract the proportionality constant for each QW sample. The polariton–exciton theory applied to 2D systems [20] correlates between this constant and the intrinsic radiative lifetime of exciton with zero crystal momentum within such a system. It has been shown that this correlation is quite robust [17] and it holds at elevated temperatures even for systems where quite large localizing potentials exist. In these cases this correlation is given by [25]

$$\frac{\partial \tau_R}{\partial T} = \frac{2M_X k_B}{\hbar^2 k_0^2} \tau_0,$$

where M_X is the exciton effective mass, k_0 is the wavevector of the photon at the excitonic resonance and τ_0 is the intrinsic radiative lifetime of the 2D system [20]. In Fig. 9 we show the intrinsic radiative lifetimes that we deduced from our measurements. We note that these times very strongly depend on the MQW width. A small dependence for QW widths which are comparable to the bulk exciton radius is expected, since τ_0 is proportional to the reciprocal excitonic oscillator strength for optical transition [20, 19]. Indeed, for GaAlAs/GaAs MQWs of 4 to 18 nm, where the bulk exciton radius is 10 nm, an increase in the intrinsic radiative lifetime of roughly a factor of two was predicted [26] and measured [19]. It is clear that in the GaN/InGaN system where the bulk exciton radius is estimated to be 3.4 nm, the increase in the intrinsic lifetimes with increasing QW width is orders of magnitude larger. Here, the built-in piezoelectric field, which separates the electron–hole pair, dramatically reduces their overlap integral and consequently their radiative lifetime increases. We estimate this effect by utilizing our $\mathbf{k} \cdot \mathbf{P}$ program to calculate the oscillator strength for optical transition across the bandgap in the presence of the 900 kV/cm electric field [11]. The solid line in Fig. 9

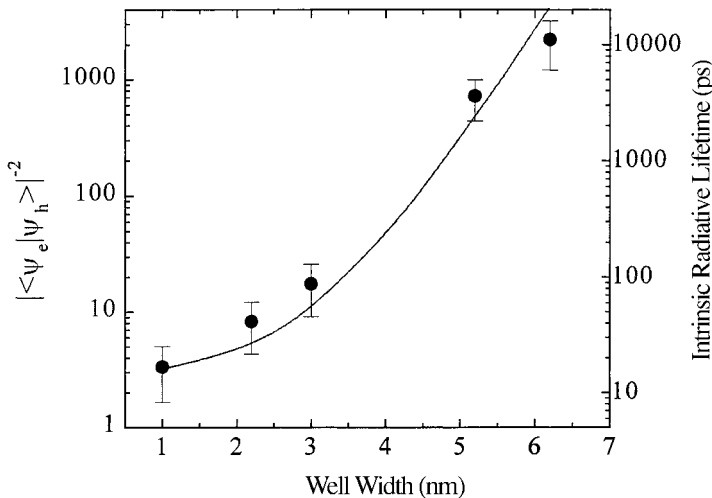


Fig. 9. Intrinsic radiative lifetimes vs. QW width. The solid line represents the reciprocal of the calculated electron-hole wavefunction overlap integral

represents the reciprocal of the calculated oscillator strength versus the MQW width. Very good agreement is obtained with the experimentally determined QW width dependence of the intrinsic radiative lifetimes.

Acknowledgement The work was supported by the Technion fund for the promotion of research.

References

- [1] S. NAKAMURA and G. FASOL, *The Blue Laser Diode*, Springer-Verlag, Berlin 1997.
- [2] I. AKASAKI and H. AMANO, *Jpn. J. Appl. Phys.* **36**, 5393 (1997).
- [3] B. GIL (Ed.), *Group III Nitride Semiconductor Compounds, Physics and Applications*, Clarendon Press, Oxford 1998.
- [4] S. NAKAMURA, *IEEE J. Select. Topics Quantum. Electronics* **4**, 483 (1998).
- [5] M.D. McCLUSKEY et al., *Appl. Phys. Lett.* **72**, 1730 (1998).
- [6] Y. NARUKAWA, Y. KAWAKAMI, S. FUJITA, and S. NAKAMURA, *Phys. Rev. B* **55**, R1938 (1997).
- [7] E. LAKIN, D. SHILO, and E. ZOLOTOYABKO, to be published.
- [8] M. LEROUX et al., *Phys. Rev. B* **58**, R13371 (1998).
- [9] S.L. CHUANG and C.S. CHANG, *Semicond. Sci. Technol.* **12**, 252 (1997).
- [10] G.A. BARAFF and D. GERSHONI, *Phys. Rev. B* **43**, 4011 (1991).
- [11] M.-E. PISTOL and D. GERSHONI, *Phys. Rev. B* **50**, 11738 (1994).
- [12] F. BERNARDINI and V. FIORENTINI, *Phys. Rev. B* **56**, R10024 (1997).
- [13] T. TAKEUCHI et al., *Jpn. J. Appl. Phys.* **36**, L382 (1997).
- [14] E. BERKOWICZ et al., in: *The Physics of Semiconductors*, Ed. D. GERSHONI, World Scientific Publ. Co., Singapore 1999 (p. 251).
- [15] I. SHTRICHMAN, D. GERSHONI, and R. KALISH, *Phys. Rev. B* **56**, 1509 (1997).
- [16] P. MICHLER et al., *Phys. Rev. B* **46**, 7280 (1992).
- [17] R. ZIMMERMANN and E. RUNGE, in: *The Physics of Semiconductors*, Ed. D.J. LOCKWOOD, World Scientific Publ. Co., Singapore 1995 (p. 1424).
- [18] D.S. CITRIN, *Phys. Rev. B* **47**, 3832 (1993).
- [19] M. COLOCCI, M. GURIOLI, and J. MARTINEZ-PASTOR, *J. Physique IV* **3**, 3 (1993).
- [20] L.C. ANDREANI, *Solid State Commun.* **77**, 641 (1991).
- [21] K.P. O'DONELL, R.W. MARTIN, and P.G. MIDDLETON, *Phys. Rev. Lett.* **82**, 237 (1999).
- [22] J. IM et al., *Phys. Rev. B* **57**, R9436 (1998).
- [23] C. WETZEL et al., *J. Appl. Phys.* **85**, 3786 (1999).
- [24] S. CHICHIBU et al., *J. Vac. Sci. Technol. B* **16**, 1 (1998).
- [25] P. LEFEBRE, J. ALLEGRE, B. GIL et al., *Phys. Rev. B* **57**, R9447 (1998).
- [26] L.C. ANDREANI and A. PASQUARELLO, *Europhys. Lett.* **6**, 259 (1988).